Published for the International Glaciological Society

THIS MANUSCRIPT HAS BEEN SUBMITTED TO THE JOURNAL OF GLACIOLOGY AND HAS NOT BEEN PEER-REVIEWED.

An Open-Source Tool for Mapping Key Metrics of Glacier Health from Space

Journal:	*Journal of Glaciology*
Manuscript ID	JOG-2026-0051.R1
Manuscript Type:	Article
Date Submitted by the Author:	n/a
Complete List of Authors:	Lamantia, Kara; University of Bristol, School of Geographical Sciences Larocca, Laura; Arizona State University, School of Ocean Futures Aberle, Rainey; US Army Engineer Research and Development Center Cold Regions Research and Engineering Laboratory Maussion, Fabien; University of Bristol, School of Geographical Sciences Lea, James; University of Liverpool, Department of Geography and Planning
Keywords:	Glacier monitoring, Glacier mapping, Remote sensing, Mountain glaciers, Glacier mass balance
Abstract:	Satellite-based observations enable monitoring of glacier health metrics, essential for assessing glacier response to climate change and the environmental services they provide. Here, we present an open-source tool for automated mapping of key climate- and mass balance-modulated parameters, including total visible ice area, snow-covered area, accumulation-area ratio, and snowline altitude. The tool uses Landsat near-infrared reflectance, commonly used spectral band ratios, and scene-specific thresholding to distinguish snow-cover from ice or firn surfaces. Validation across 59 glaciers spanning 13 regions shows strong agreement with manual interpretation of satellite imagery and weak agreement with field observations from the World Glacier Monitoring Service (WGMS) likely reflecting differences in methodology, observation timing, and the transient nature of glacier surface conditions. While the tool increases the availability of glacier observations beyond those

	provided by WGMS, these metrics should be interpreted as complementary transient observations rather than direct substitutes for end-of-season or field-based measurements. Beyond the glaciers studied here, the tool is designed to enable accessible generation of multi-decadal glacier health time series for individual glaciers with appropriate user evaluation and consideration of known limitations. Thus, the tool will hold value for a range of users, particularly for education, outreach, and community stakeholders.

An Open-Source Tool for Mapping Key Metrics of Glacier Health from Space

Kara A. Lamantia[1*], Laura J. Larocca[2*], Rainey Aberle[3], Fabien Maussion[1], James M. Lea[4]

[1]School of Geographical Sciences, University of Bristol, Bristol, UK
[2]School of Ocean Futures, Arizona State University, Tempe, AZ, USA
[3]Cold Regions Research and Engineering Laboratory, Hanover, NH 03755, USA
[4]Department of Geography and Planning, University of Liverpool, Liverpool, UK

*These authors contributed equally to this work

Correspondence: Kara Lamantia <kara.lamantia@bristol.ac.uk>

Abstract

Satellite-based observations enable monitoring of glacier health metrics, essential for assessing glacier response to climate change and the environmental services they provide. Here, we present an open-source tool for automated mapping of key climate- and mass balance- modulated parameters, including total visible ice area, snow-covered area, accumulation-area ratio, and snowline altitude. The tool uses Landsat near-infrared reflectance, commonly used spectral band ratios, and scene-specific thresholding to distinguish snow-cover from ice or firn surfaces. Validation across 59 glaciers spanning 13 regions shows strong agreement with manual interpretation of satellite imagery and weak agreement with field observations from the World Glacier Monitoring Service (WGMS) likely reflecting differences in methodology, observation timing, and the transient nature of glacier surface conditions. While the tool increases the availability of glacier observations beyond those provided by WGMS, these metrics should be interpreted as complementary transient observations rather than direct substitutes for end-of-season or field-based measurements. Beyond the glaciers studied here, the tool is designed to enable accessible generation of multi-decadal glacier health time series for individual glaciers with appropriate user evaluation and consideration of known limitations. Thus, the tool will hold value for a range of users, particularly for education, outreach, and community stakeholders.

1. Introduction

Mountain glaciers and seasonal snowpacks act as crucial freshwater reservoirs, supplying water for irrigation, hydroelectric generation, and a wide range of ecosystem services (e.g., Immerzeel and others, 2020). In recent decades, Earth's glaciers have been losing mass at an accelerated rate, marking a retreat unprecedented in at least the last two thousand years (e.g., Hugonnet and others, 2021; Masson-Delmotte and others, 2021; Calvin and others, 2023, Larocca and others, 2023). Community estimates of global glacier mass changes since 2000 suggest that glacier mass loss is ~18% greater than that of the Greenland Ice sheet (-262 Gt yr^{-1} 2002-21 versus -223 yr^{-1} 2002-20, respectively) and more than twice that from the Antarctic Ice Sheet (-111 Gt yr^{-1} 2002-20; Otosaka and others, 2022; The GlaMBIE Team, 2025). By 2100, global-scale projections estimate that glaciers will lose 26–41% of their mass relative to 2015, with 49–83% projected to disappear entirely (Rounce and others, 2023).

Glacier mass balance monitoring is vital for local hazard impact assessments and global climate projections (e.g., Haeberli and Whiteman, 2015; Huss and Hock, 2018; Hock and others, 2019; Hugonnet and others, 2021; Rounce and others, 2023; Ficetola and others, 2024). Notably, the major source of uncertainty in predicting near-term glacier change (i.e., to the mid twenty-first century) lies not in the emission scenario, but in the glacier models themselves (Marzeion and others, 2020; Schuster and others, 2023). These uncertainties arise in part from varying model sensitivities to air temperature and precipitation, which respectively regulate ablation and accumulation processes (Meier, 1962; Braithwaite

& Müller, 1980). As a result, improving the availability and use of observational constraints is critical for reducing uncertainty in glacier projections and their associated impacts (e.g., Wells and others, 2025).

The Randolph Glacier Inventory (RGI; RGI 7.0 Consortium, 2023) is the most widely used and globally complete glacier observational dataset, on which most global-scale projections rely to define initial condition or reference state (e.g., Hugonnet and others, 2021; Rounce and others, 2023; The GlaMBIE Team, 2025). Although recently updated in 2023, the RGI represents a snapshot of the world's glaciers with a reference date of the year ~2000 (Fig. 1; Pfeffer and others, 2014; RGI Consortium, 2023). In the ~25 years since then, global temperatures have continued to rise, leading to major changes in glacier length, area, and volume worldwide (Rounce and others, 2023). As such, many glaciers have now retreated within their RGI-defined boundaries, and some have disappeared entirely (e.g., Ramírez and others, 2001; Huss at al., 2025; Van Tricht and others, 2025; Baruah and others, 2026; Serrano and others, 2026). Thus, globally consistent, time-varying glacier observations needed for glacier model calibration and evaluation are largely lacking to date.

Less than 0.2% (<500) of the world's >200,000 glaciers are monitored in situ (WGMS, 2023). Satellite-based observations offer a means to monitor key metrics of glacier health over much broader spatial scales (e.g., Rastner and others, 2019; Aberle and others, 2025). However, challenges such as cloud cover, topographic shadowing, and spectral similarities between snow, ice, and firn have complicated monitoring efforts across Earth's diverse glacierized settings (e.g., Rastner and others, 2019, Racoviteanu and others, 2019; Aberle and others, 2025). To address some of these challenges and expand accessible space-based observations of glacier state, we developed a user-friendly, open-source Google Earth Engine (GEE) tool that enables users to automatically quantify several indicators of glacier health from the year 1985 to present. Here, we use the term "glacier health" to refer to a range of indicators: total visible ice area (TA), snow-covered area (SCA), snowline altitude (SLA), and accumulation-area ratio (AAR). These glacier surface variables are observable from satellites and are closely linked to climate and surface mass balance processes.

To validate the tool, we compared our satellite-based observations (a total of 1,531 observations spanning 40 years) for a set of 59 glaciers with (1) long-term in situ field-based measurements from the World Glacier Monitoring Service (WGMS, Fig. 1), and (2) manual digitizations of end of season SCA and TA. These new data will enable direct comparisons between satellite-derived and modeled glacier-specific metrics, local climatological data, and glacier morpho-topographic variables, offering much-needed insights into glacier-climate sensitivity across diverse climate and topographic settings. The tool will also facilitate broader use of these data by non-specialist users, including educational applications.

Figure 1 near here.

2. Methods

2.1. Glacier health metrics

We focus on the following four glacier health metrics which capture changes in glacier geometry and surface facies (e.g., snow-, firn- and ice-covered areas) in response to local climatic controls on accumulation and ablation (Fig. 2):

(1) snow-covered area (SCA, km^2), representing the zone of accumulation where mass gained via annual snowfall exceeds melting;

(2) snowline altitude (SLA, m), defined as the lower limit of the SCA or the average elevation of the transition between snow-covered and ice- or firn-covered (ablation zone) surfaces (Cogley and others, 2011). When measured at the end of the balance year (and given no superimposed ice zone), the SLA may be used as a proxy for the equilibrium line altitude (ELA; e.g., Rabatel and others, 2012. 2013; Larocca and others, 2024), the elevation at which the annual net mass balance is zero (Cogley and others, 2011);

(3) total visible ice area (TA, km^2), representing the spatial extent of the glacier (i.e., bare ice area plus snow area, not accounting for debris covered ice); and

(4) accumulation-area ratio (AAR, unitless), defined as the ratio of the accumulation area (SCA) to the TA, for debris-free glaciers. As adjustment of glacier geometry (i.e., TA) is lagged relative to climate forcing, the AAR can indicate the extent of imbalance relative to current climatic conditions (Benn & Evans, 2010).

Figure 2 near here.

2.2. Study glaciers

For the analyses presented here, we derived the four glacier health metrics for a set of 59 well-monitored glaciers with long-term, field-based mass-balance observations archived by the WGMS (referred to hereafter as study glaciers; Fig. 1 and SI Table 1). This set represents a subset of the 70 glaciers reported by Ohmura and Boettcher (2022), selected based on data quality, duration of observations (i.e., those with multi-decadal annual mass-balance records), suitability for satellite-based analysis (i.e., outside Antarctica), and size (i.e., large ice caps were excluded). Within these 59 study glaciers there are 45 land-terminating and 15 lake-terminating glaciers (defined as having a lake inside or intersecting the RGI boundary). We also note that none of the 59 study glaciers exhibit extensive debris cover.

All metrics were measured annually between 1985 and 2024 using a single satellite image per glacier and year, selected within a ±1 month window centered on the month best approximating the end of the ablation season for each location (we note that in some years, a suitable image was not available for every glacier; see Section 2.3 and SI Table 1). The target month was approximated based on region and the average survey month from which WGMS data is available. Although this sample represents only a small fraction of the world's glaciers, the selected glaciers span a wide range of geographic and climatic settings and are distributed across 13 of the 19 first-order regions defined by the RGI (Fig. 1; RGI Consortium, 2023). The subsequent validation focuses on this subset of well-observed glaciers, while the underlying methodology of the tool is designed with the broader goal of being applicable to any glacier or glacier complex within the RGI (without extensive debris cover; see Section 2.3 and 4.3).

2.3. Cloud-based satellite imagery analysis

Our workflow (Fig. 3), implemented in GEE, integrates satellite imagery across multiple sensors (Landsat 5, 7, 8, and 9) to automatically derive annual glacier-specific health metrics across a 40-year period (SI Table 2). To avoid introducing additional complexity associated with integrating imagery from multiple satellites with different spatial resolutions and spectral characteristics, we limited the workflow to Landsat imagery, which has the unique advantage of multi-decadal temporal coverage (e.g., Sentinel-2 was not included because it lacks a thermal band used in our water-masking approach, while the coarse spatial resolution of MODIS is insufficient for many of the glaciers considered here). While Landsat imagery is available beginning in 1984, we chose to set our observation start year to 1985, as most study glaciers did not have sufficient imagery in 1984. Specifically, the algorithm integrates terrain-corrected multispectral Landsat imagery with established spectral indices, e.g., the Normalized Difference Snow Index (Dozier, 1989; Riggs and others, 1994; Hall and Riggs, 2010), band ratios, and automated thresholding techniques (Otsu segmentation; Otsu, 1979) to characterize glacier surfaces (i.e., to delineate snow versus ice or firn), as described below.

Figure 3 near here

A single image per year is selected to maintain computational feasibility within GEE. Processing and/or rendering multiple images per year frequently exceeded GEE memory limits, resulting in task failures and timeouts. In addition, recent changes to GEE's noncommercial usage model have introduced quotas that further limit large-scale analysis. Therefore, although our workflow aims to identify the 'best' image within the target month (i.e., the month best representing end-of-ablation season conditions, ideally prior to accumulation season snowfall events), we recognize that the selected image may be acquired up to several weeks before or after the true end of the mass-balance year. To select a single image per glacier and year, we use a two-step procedure that balances image quality with seasonal representativeness.

Landsat scenes are first identified within a ±1 month window centered on a target month. To prioritize the target month, the algorithm first searches within the target month only using a strict cloud-cover criterion (user-defined maximum cloud cover minus 5 percentage points). If one or more scenes meet this criterion, the least-cloudy target-month scene is selected for that year. If no target-month scene meets the criterion, the algorithm falls back to the broader ±1 month window and selects the least-cloudy scene meeting the user-defined maximum cloud-cover threshold (Fig. 4). For example, if August is the target month and the maximum allowable cloud cover is 20%, the workflow preferentially selects August scenes with cloud cover ≤15%; if none are available for a given year, it selects the best available scene from July or September (≤20%). This approach increases the fraction of target-month acquisitions while limiting increases in average scene cloudiness. We note that Landsat 7 imagery acquired from 2003 onwards are excluded due to data gaps associated with the Scan Line Corrector failure, rendering them unsuitable for use in our analysis. Maximum cloud cover and minimum sun angle were set to 20% and 20°, respectively, for the 59 glaciers studied.

Cloud cover is assessed from the QA_PIXEL band, where Bit 3 stores the high-confidence cloud flag from the CFMask algorithm (Zhu and others, 2015). A binary mask of flagged pixels within the glacier boundary is used to estimate the percentage of cloud covered pixels (and this value is appended to the output file as *cloud_pct_roi*). However, this mask is known to perform poorly over snow- and ice-covered terrain because these bright, highly reflective surfaces can be difficult to distinguish from clouds, often resulting in cloud-cover estimates that are biased high over glacierized regions (Stillinger and others, 2019). Therefore, we retain *cloud_pct_roi* metadata as a diagnostic flag and suggest that users use this information to identify and evaluate potentially problematic observations.

Following selection of annual images and using a chosen digital elevation model (DEM), the Ekstrand correction (Ekstrand, 1996), a topographic normalization technique, is applied to account for illumination differences arising from sun elevation, incidence angle, and terrain shadowing, typical of mountainous glacierized environments (SI Fig. 1). After terrain correction, a masking procedure adapted from Moussavi and others (2020) is applied to reduce misclassification from surrounding rock and water surfaces. The masking is based on a thermal infrared–to–blue band reflectance ratio combined with a blue reflectance threshold. Because the original masking approach was optimized for seawater, and glacial lakes are often brighter due to suspended rock flour, multiple threshold combinations were evaluated to balance removal of surrounding rock and glacial lakes while minimizing over-masking of true snow and ice glacier surfaces. Masking options are classified as *light, moderate,* or *high* where the thermal-to-blue reflectance ratio threshold and blue thresholds are set at >0.9 and <0.1, >0.9 and <0.2, and >0.85 and <0.2, respectively. In general, the *moderate* threshold was found to be most effective for our study glaciers (see Section 2.4; SI Fig. 2). Thus, in most cases masking was set to the *moderate* option or to *Off* (the former for study glaciers that terminate in or near a lake; see SI Table 1). The *light* and *high* options are intended for cases in which the *moderate* option either over-masks glacier surfaces or under-masks rock and water features, respectively.

Figure 4 near here.

Once masked and terrain-corrected, each image is used to derive the four primary metrics of glacier health: SCA, SLA, TA, and AAR. TA is calculated using a dual-threshold approach combining the NDSI >0.4 and a near-infrared (NIR)–to–shortwave infrared (SWIR) reflectance ratio (NIR/SWIR1 >1.4) to distinguish snow- and visible ice-covered glacier area from water, rock, and bare earth surfaces. Next, the SCA is derived from the TA using Otsu's thresholding method applied to terrain-corrected NIR reflectance (Fig. 5a). This approach identifies an image-specific reflectance threshold from each NIR histogram and is used to distinguish snow-covered from bare ice pixels within the previously defined total glacier area (Fig. 5b; Otsu, 1979; Rastner and others, 2019). Importantly, this approach extends beyond the limitations of visible light by exploiting contrasts in NIR reflectance where snow reflects strongly and bare ice is more absorptive (Warren, 2019). This allows snow-covered and bare ice boundaries to be identified even when they are not visibly discernible. Moreover, the Otsu-derived threshold is image-specific, avoiding reliance on a fixed reflectance threshold that may not perform consistently across different images and glacier settings. The Otsu thresholding approach assumes a bimodal NIR reflectance distribution. However, this assumption may not hold for images acquired during or shortly after snowfall events, where the glacier surface is mostly or fully snow-covered and thus the secondary peak may be weak or absent. Such cases may result in anomalously high or low snowlines. To identify these cases, the workflow evaluates the histogram's shape and returns one of four quality flags (*'ok', 'secondary peak too small', 'class imbalance',* or *'empty histogram'*), which are written to the output file. This enables the user to identify and remove years of anomalous snowlines. These flags are intended as diagnostic information to support post-processing and quality control (i.e., images are retained in the final export rather than being automatically excluded from analysis).

Glacier areas (TA and SCA) are calculated by summing classified pixels multiplied by pixel area (30 m resolution) and are reported in square kilometers. Next, the AAR is calculated as the ratio of the SCA to the TA. Finally, the SLA is determined by identifying the glacier elevation that corresponds to the fraction of glacier area lying below the snowline (i.e., 1 − AAR). For example, for a glacier with an AAR of 0.6, the SLA corresponds to the elevation at which 40% of the total glacier area lies below, equivalent to the 40th percentile of the glacier's area–elevation distribution. We note that in the case where the entire glacier surface is ice-covered (i.e., AAR = 0), the SLA will correspond to the 100th percentile of the glacier's area-elevation distribution. Our approach is conceptually similar to that of Krajčí and others (2014) hypsometrical approach as well as the snow-cover classification workflow in Aberle and others (2025). Other approaches using optical imagery have derived SLA from manual delineation in true or false-color image composites (e.g., Rabatel and others, 2013; Larocca and others, 2024), from the lowest two percentiles of the snow-covered surface (Loibl and others, 2025), or from the lowest elevation bin within a sequence that is >50% snow-covered (Rastner and others, 2019). We adopted a hypsometric approach because the snowline is often irregular, and discontinuous or patchy, and is therefore commonly represented as a zone rather than a discrete line (e.g., Rastner and others, 2019). Deriving SLA from the elevation distribution provides an estimate of snowline elevation that does not rely on explicit delineation of individual snowline boundary pixels. However, we note that because SLA is derived from AAR, which itself depends on the classification of the glacier surface, uncertainties in the surface classification propagate into the resulting SLA estimates.

We evaluated the sensitivity of our results to the choice of SLA derivation approach by comparing our approach against four alternative methods: (1) the minimum elevation of snow-covered pixels (*Lowest Snow*), (2) the lowest elevation bin containing at least 75% snow cover, with a fallback threshold of 60% if 75% was not reached (*Band*), (3) the elevation at which snow cover within elevation bands crosses 50% (*Transition50*), and (4) the elevation at which snow cover within elevation bands crosses 75% (*Transition75*). Relative to our approach, the *Lowest Snow* method produced substantially lower SLAs (median difference = −175 m), whereas the other methods yielded comparatively small differences (median differences of −14, −31, and +13 m, respectively; SI Fig. 3). These results suggest that the choice of SLA definition introduces relatively modest uncertainty compared to other limitations, such as image acquisition timing. Furthermore, the strong agreement between our automated and manually derived SLAs suggests that the selected method provides a reasonable approximation of the snow–ice/firn transition. We additionally note that because the timing of minimum snow cover can vary by several weeks (e.g., Aberle and others, 2025), SLAs derived from a single annual image should be interpreted as a transient observation and likely do not capture the true end-of-season ELA.

Elevations used in the study glacier SLA calculations were obtained from either the ArcticDEM (2 m mosaic; Porter and others, 2023) or the Copernicus GLO-30 DEM (COPDEM; European Space Agency, 2024), depending on data availability for each glacier location (SI Table 1). Both products are multi-temporal composites with acquisition periods spanning ~2007-2024 and ~2010-2015, respectively.

The tool also contains an option to use the 30 m NASADEM (Crippen and others, 2016) released in 2020 and based on a reprocessing of Shuttle Radar Topography Mission radar data acquired during an eleven-day window in 2000. To assess the sensitivity of the derived metrics to DEM choice, glacier health metrics were generated for a subset of 23 glaciers with coverage from both COPDEM and NASADEM. The resulting differences are discussed in Section 4.2. Extracted data for the 59 study glaciers include annual glacier metrics, satellite imagery metadata, all imagery flags, TA and SCA area-elevation distributions, and annual TA and SCA shapefiles.

Figure 5 near here.

2.4. The Graphical User Interface

The graphical user interface (GUI) allows users to specify key processing parameters, enabling customization of the workflow for individual glaciers with step-by-step instructions available via a GitHub repository (see Data Availability Statement). Upon loading, the GUI prompts the user to select either the RGI glacier product or the RGI glacier complex product (Step 1). The latter product is new to RGI v7.0 and merges connected glaciers into one entity, while in the former, individual glaciers are represented separately (RGI Consortium, 2023). The RGI glacier product is also available through the GEE Community Catalog if the user prefers loading the dataset themselves. Further information about accessing the GEE Community Catalog dataset is located in the Data Availability statement and through the GUI's GitHub documentation.

Once the selected dataset is loaded, the GUI enables the user to select the glacier of interest by clicking within its boundary (Step 2). Clicks outside a glacier outline trigger an error notification indicating that no glacier has been selected, prompting the user to repeat the selection. Once selected, the algorithm highlights the glacier of interest, and a default 50 m buffer is applied to the glacier outline. This buffer can be adjusted by the user from 0 to 200 m in 50 m increments. To prevent inclusion of areas belonging to neighboring glaciers, outlines are clipped along shared boundaries, such that buffering is applied only to boundaries unique to the glacier of interest. Since the RGI represents a temporal snapshot of global glacier extent centered roughly around the year 2000 and our workflow derives glacier health metrics beginning in 1985, the buffer ensures the inclusion of ice outside the RGI margins during years prior to the outline source date.

In the GUI (SI Fig. 4) the left panel provides user controls for specifying imagery acquisition parameters (*Collect Imagery*) and processing options (*Processing Options*; Table 1). Required inputs for imagery collection include a glacier name or ID (used for export file naming), the start and end years of interest, a target month (1–12; typically corresponding to the month best representing the end of the melt season), the maximum allowable cloud cover (0–100%), and the minimum sun angle (0–90°). By default, the maximum end year corresponds to the most recent year of available imagery (e.g., 2026, at present). Once imagery is collected (Step 3), the console (right panel) reports the total number of candidate images (i.e., images that meet the user-defined criteria), as well as metadata (cloud-cover percentage) for the annually selected images, chosen as the least-cloudy scene. The map view displays the glacier outline as the region of interest (ROI) and the earliest annually selected image rendered in true color (RGB). We note that imagery acquisition parameters can be modified, and the procedure repeated, to evaluate alternative image selections under different criteria.

Following imagery selection, users specify the DEM (either the COPDEM, NASADEM, or ArcticDEM) and the rock/water masking strength under *Processing Options*. A validation check confirms that the selected DEM covers the ROI (Step 4). The rock/water masking (Step 5) is then chosen using one of three predefined levels: *light*, *moderate*, and *high*, corresponding to progressively stricter masking or disabled if not required using the *Off* option (SI Fig. 2). Once *Run Analysis* (Step 6) is initiated, the algorithm is executed using the specified parameters for all selected years. Derived glacier health metrics for the first annually selected image are reported within a feature collection in the console, and the corresponding SCA and TA masks are displayed in the map view. The analysis can be re-run after modifying the selected parameters. Each new execution refreshes the map layer, and new results are reported in the console. When glacier metrics for a given year require further inspection (e.g., appear anomalous or are flagged), the user may enter that year as the 'start year' to view the corresponding imagery in the map view. All outputs generated by the analysis are listed in the Tasks tab and can be run to export results to Google Drive (Step 7). Outputs include (1) a CSV file containing annual glacier metrics (TA, SCA, AAR, and SLA), uncertainties, imagery flags, and satellite imagery metadata, (2) annual TA and SCA polygon shapefiles (Fig. 5b), and (3) CSV files containing annual TA and SCA area-elevation distributions (i.e., pixel counts aggregated into 50 m elevation bins).

Table 1 near here.

2.5. Tool validation and uncertainty

To evaluate the performance of the GEE-based tool (hereafter we use *tool*) and estimate uncertainty, we compare annual glacier health metrics derived from the tool with observations from the WGMS and with manually digitized data for the 59 study glaciers. Specifically, tool-derived metrics are compared with the following annual WGMS field-measured observations when available (from the 2024 Fluctuations of Glaciers Database *mass_balance_overview.csv* and *mass_balance.csv* files; WGMS, 2024*)*: ELA (mean elevation averaged over the glacier of the end-of-mass-balance-year equilibrium line, m), accumulation area (km^2), ablation area (km^2), and annual balance (mass balance over the hydrological year, mm w.e. ~ kg m^{-2}). We also compute WGMS TA (km^2) as the sum of the accumulation and ablation areas and WGMS AAR (unitless) as the accumulation area divided by the TA. We assume annual WGMS observation dates from the survey date (YYYYMMDD) in the *state.csv* file when available.

To provide an independent benchmark for evaluating tool performance, manual digitizations were conducted for a subset of glacier–year combinations. For each of the 59 study glaciers, four Landsat scenes were randomly selected from the set of images analyzed by the tool. Using these images (n = 236) and their corresponding RGI outlines, SCA and TA were manually delineated as polygons using false-color Landsat imagery (NIR–red–green composites; SI Fig. 5). SLA was subsequently calculated from the manually digitized polygons using the same DEM-based percentile method applied in the tool workflow, and AAR was calculated as the ratio of manually derived SCA to TA.

Tool performance was quantified using the mean bias, root-mean-square error (RMSE), mean absolute error (MAE), and Pearson correlation coefficient (r) between tool-derived and reference values (WGMS and manual). Uncertainty in tool-derived glacier health metrics was defined from comparisons with manual digitizations only (see Section 4.1). Specifically, for each metric, uncertainty was quantified as the median absolute percent difference between tool-derived and manually digitized values across all glacier–year pairs. The resulting values are applied as fixed percentage uncertainties for all tool-exported values. For example, a tool-derived TA (±5%) of 50 km^2 is reported with an uncertainty of ±2.5 km^2, while a TA of 10 km^2 is reported with an uncertainty of ±0.5 km^2 (see Results 3.1).

In addition, we assess and compare tool- and WGMS-derived changes in glacier health metrics over the 40-year period across the 59 study glaciers and compare tool-derived metrics with annual mass balance from the WGMS. Because the study glaciers differ in size, geometry, and climatic setting, TA and SCA values are normalized within each glacier relative to the median of all available observations within the 1985–2024 period. Values are expressed as percent change relative to this baseline and summarized across glaciers for each year using the median and interquartile range (IQR). SLA/ELA data are analyzed as anomalies relative to the same baseline period. Lastly, to quantify how well our tool-based observations complement, rather than replace, WGMS field-based monitoring, we assess the increase in temporal observational coverage provided by the tool for the same glaciers.

3. Results

3.1 Post processing

Application of the tool to the 59 study glaciers resulted in 1,531 observations over the 40-year period. To remove observations potentially affected by snowfall, cloud cover, or shadowing that were not excluded during the initial imagery collection process, we applied a glacier specific quality-control filter based on scatterplot smoothing (LOESS). Because SCA, SLA, and AAR can exhibit substantial interannual variability, whereas TA is expected to evolve more gradually (i.e., as a lagged response to climate), TA was used to identify anomalous observations within our dataset. For each glacier, a LOESS curve (frac = 0.45) was fitted to the TA time series to estimate the glacier's trajectory through time. Residual variability about the fitted curve was quantified using the median absolute deviation, scaled to an equivalent standard deviation. Glacier-years with residuals exceeding ±2.5 standard deviations were flagged and removed (SI Fig. 6). This resulted in the removal of 176 observations (11.5%), bringing our observation total to 1,355. The study glaciers were binned into equally distributed size categories (small: 0.04 – 2.97 km^2, n=20; medium: 2.98 – 9.09 km^2, n=20; large: >9.1 km^2, n = 19) and the filtering rates were broadly similar across glacier size categories (small: 11.1%, medium: 14.7%, large: 6.9%). We note that we did not remove any additional observations based on imagery flags (e.g., the NIR histogram or cloud cover assessment).

3.2 Tool validation and uncertainty

SLA/ELA shows the strongest agreement among the four metrics for the tool-derived–WGMS comparisons (r = 0.99; SI Fig. 7). However, the relationship is weak when SLA/ELA values are expressed as an anomaly relative to each glacier's median tool-derived SLA (r = 0.20; Table 2 & Fig. 6). A negative bias (−112 m) suggests that tool-derived SLAs are, on average, lower than WGMS ELAs. Restricting the comparison to observations acquired within ±7 days of the WGMS survey date reduced the mean SLA bias from –112 m to –61 m, indicating that acquisition timing contributes to the observed discrepancy. Tool-derived estimates of SCA and TA also agree well with WGMS observations of accumulation area (r = 0.90) and total area (computed as the sum of the reported accumulation and ablation areas; r = 0.97), in absolute terms, but correlations are weak when values are normalized to account for between-glacier differences in size (r = 0.26 and r = 0.22, respectively). Mean biases suggest the tool generally overestimates SCA and TA relative to WGMS (+ 2.1 km^2 and + 0.4 km^2, respectively). Because glacier size varies across the study sample, we also report median absolute percent differences of 46% for SCA and 9% for TA.

Comparison with manually digitized data demonstrates stronger agreement across all glacier health indicators (Table 2 & Fig. 6). Tool-derived SLA shows a strong correlation with manual SLA estimates in absolute terms (r = 0.99) and when values are expressed as anomalies (r = 0.73), with a bias of 18.5 m and an RMSE of 83.3 m. SCA and TA also show good agreement with manual observations (e.g. four randomly selected images per glacier; SI Fig. 5) in absolute terms (r = 0.98 and r = 0.99, respectively) and when values are normalized to account for between-glacier differences in size (r = 0.73 and r = 0.59, respectively). Biases of −1.0 km^2 and −1.5 km^2 indicate an underestimation of SCA and TA relative to manual delineations. Based on comparisons with manual delineations, typical relative uncertainties (derived from median absolute percent differences) in the tool-derived metrics are estimated to be ±1% for SLA, ±10% for SCA, and ±5% for TA. We also compare per-glacier WGMS- and tool-derived glacier health metrics (TA, SCA and SLA/ELA) with WGMS records of annual mass balance (Fig. 7 and SI Fig. 8). Median per-glacier Pearson correlation coefficients (r) are TA (r = 0.43, 0.39), SCA (r = 0.37, 0.88), and SLA/ELA (r = −0.30, −0.89), for the tool and WGMS, respectively. The tool performs well relative to manual delineations; however, we note that agreement is overall weak for tool–WGMS comparisons. This could be due to a variety of reasons including methodological and data acquisition date differences between the two datasets (see Discussion 4.1.).

Table 2 near here.
Figure 6 near here.

3.3. Change in glacier area over time

Across the 59 study glaciers, both the tool-derived and WGMS observations indicate substantial long-term changes in glacier area (Fig. 7). Linear regression of annual median values (summarized across glaciers) indicates a tool-derived decline in SCA of 8% per decade ($p < 0.001$), corresponding to a total decrease of ~30% over the four-decade study period. In contrast, WGMS observations indicate a much stronger decline of 14% per decade ($p < 0.001$), equivalent to a ~54% reduction. TA shows a more gradual decline and better agreement between datasets, with trends of −5% per decade ($p < 0.001$; total −20%) and −3% per decade ($p < 0.001$; total −13%) for the tool and WGMS, respectively.

Temporal trends in SCA derived from WGMS observations are steeper than those derived from the tool, likely reflecting differences in observation timing within the ablation season between the two datasets (see Discussion section 4.1.). Despite these differences, both datasets indicate declining glacier areas (with changes in TA occurring more slowly relative to changes in SCA) between 1985 and 2024. Considering all glacier–year combinations across the 59 study glaciers and 40-year period (2,360 potential observations), the tool returns results for ~65% of cases (1,531 observations). In total, the tool yields 803 and 206 additional observations of SCA and ELA, respectively, substantially increasing the total number of available observations.

Figure 7 near here.

4. Discussion

4.1. Interpreting differences between satellite-derived and field observations

Overall, the tool reliably captures glacier surface conditions from optical satellite imagery and agrees well with manually derived metrics (see Section 3.1.) supporting the underlying methodology and the use of the tool for generating transient observational data for unmonitored glaciers. However, we observe a weak overall agreement between the tool-derived glacier health metrics and WGMS records. We suggest that this is likely reflective of methodological differences and temporal mismatches between the satellite-derived and field-based observations.

WGMS observations are compiled from a global network of investigators and are primarily obtained using distributed ablation stakes and snow pits taken as point measurements and inter-/extrapolated across the glacier surface, from which quantities such as ELA and AAR are derived (Zemp and others, 2009). Survey platform methods for WGMS measurements of glacier length, area, and elevation range also vary between investigators and glaciers (e.g., terrestrial, airborne, spaceborne). In contrast, the tool derives annual space-based glacier health metrics from spatially continuous classifications of glacier surface conditions. Additionally, we use the RGI v7.0 outlines with a 50 m buffer applied. Although this likely captures past (pre-2000) glacier extents, the resulting maximum boundary is fixed in time and does not account for any extents beyond this boundary.

Field-based surveys are typically conducted near the end of the mass-balance year, usually at the end of the ablation season when the mass of the glacier is at the annual minimum (Cogley and others, 2011). In comparison, the tool relies on a single annual satellite image selected to best approximate end-of-ablation season conditions. However, accurately capturing end of the ablation season conditions is limited by Landsat's revisit interval (i.e., temporal resolution of ~16 days), frequent cloud cover, and GEE memory limitations, which restricts the ability of the tool to analyze multiple images per year. As a result, WGMS observations are not directly comparable with single-date satellite observations which capture transient conditions. The mean temporal offset, Tool − WGMS, is ~20 days (SI Fig. 9), however we note that this could be further reduced with the use of multiple satellites. Thus, our comparisons may involve non-coincident observations (e.g. a mid-September satellite image compared with a late-August field survey), and tool observations were, on average, acquired later than the corresponding field observations. Further, in years with late-summer or early-fall snowfall events, satellite scenes may depict snow-covered glacier surfaces that do not represent true end-of-balance-year conditions. Our workflow aims to identify images in which the glacier is fully snow-covered through analysis of the NIR band's histogram. However, this approach produced mixed results in its ability to flag snowy images (SI Fig. 10). While the NIR histogram assessment can be useful for identifying potentially problematic scenes and guiding visual inspection, it should be interpreted with caution and not as a definitive indicator of image or classification quality.

These temporal mismatches are most problematic for variables that rely on the position of the snowline (ELA/SLA, SCA, and AAR) as it migrates through the melt season (e.g., Mernild and others, 2013). This limitation has been noted in other studies that have mapped snow extent on glaciers using multi-temporal Landsat satellite imagery (e.g., Rastner and others, 2019; Larocca and others, 2024). In addition to these temporal limitations, we note that the SLA is not always strictly equivalent to the ELA (i.e., in cases where there is a superimposed ice zone; Cogley and others, 2011). We also note that for comparisons to the mass balance data, it is natural the WGMS dataset has a much higher agreement as the mass balance dataset is supplied through the WGMS database, reflecting internal consistency and not necessarily independent validation.

The data provided by the WGMS are geographically biased to the Northern Hemisphere and are subject to occasional errors, inaccuracies, and missing metadata (e.g., Zemp and others, 2009; Ohmura and Boettcher, 2022). The set of glaciers used to evaluate the performance of the tool reflect this same uneven global distribution, as they were selected from the small subset of glaciers worldwide that possess long-term field-based records. In a review of the worldwide monitoring network, Zemp and others (2009) suggest that WGMS data may contain difficult-to-quantify systematic and random errors and that these data should therefore be quality-checked against related literature prior to use. In our analysis, obvious errors (e.g. misplaced or missing decimal points and reported zeros in accumulation area with ELAs below the glacier's maximum elevation) were corrected or excluded (we note that in the latter case the reported ELAs were retained) where possible before comparison with the satellite-derived data. Zemp and others (2009) also suggest that the accuracy of the summer balance and ablation-area observations generally exceeds that of the winter balance and the accumulation-zone observations.

In summary, interpretation of the differences between the WGMS and tool-derived observations requires consideration of both methodological differences and uncertainties in the two datasets. For instance, WGMS observations are derived from field surveys that differ in survey method, spatial coverage, and the approach used to determine ELA and its elevation. In contrast, the tool derives SLA from satellite imagery using a DEM-based hypsometric approach and is influenced by DEM choice, image acquisition timing, and the transient nature of glacier surface conditions (see Section 4.2.). Together, these methodological differences and uncertainties likely contribute to the observed biases between the datasets, although disentangling their relative contributions is not possible given the likely variability in WGMS field data collection methodologies between individual glaciers.

4.2. Tool limitations and design choices

The spectral characteristics of seasonal snow, glacier ice, and firn are similar in optical satellite imagery, with the reflectance signatures of snow and firn exhibiting the greatest overlap (e.g., Fig. 1 in Aberle and others, 2025). This similarity can complicate glacier snow cover mapping because misclassification of firn as snow can lead to an overestimation of the seasonal snow-covered area and an underestimation of the ELA/SLA. In such cases, the inferred boundary will correspond to the firn-ice boundary rather than the true snow-firn boundary (e.g., Fig. 10 in Aberle and others, 2025). Although snow and firn can also be visually difficult to distinguish in moderate-resolution (30 m) imagery (e.g., Rabatel and others, 2013; Larocca and others, 2024), we suggest that the larger bias between satellite-derived SLAs and field-measured ELAs (Table 2: −112 m), together with the lower bias between satellite- and manually derived SLAs (18.5 m), indicates that in some cases the tool did not capture true end-of-ablation-season conditions rather than reflecting a systematic classification error of firn as snow.

As noted above and in section 4.1., the most important limitation of the tool is the low temporal sampling frequency (i.e., the use of only one image per year) in highly dynamic glacier environments. Our workflow is intentionally designed around this single-image approach for reasons of computational feasibility in GEE, and thus, is a deliberate trade-off considering the accessibility that GEE provides. By limiting computational demands, the tool is designed to maximize accessibility and ensure usability across a range of GEE account types. SCA, AAR, and SLA are not static annual properties but transient surface conditions whose interpretation depends strongly on acquisition timing. Glacier snow cover and SLA can change substantially over short time periods during the ablation season and early in the accumulation season, and thus a single acquisition can be strongly affected by recent snowfall, transient melt conditions, cloud contamination, cloud shadows, terrain shadow, or local scene-specific illumination effects (Rastner and others, 2019; Mernild and others, 2013). Thus, we suggest that the tool derived metrics should be viewed as transient observations rather than observations representative of end-of-melt-season conditions.

An additional limitation is that our algorithm does not employ a time-varying DEM (as, to date, these data are not readily available) and instead uses either the ArcticDEM, COPDEM, or NASADEM depending on the glacier location and user choice. Consequently, our approach does not account for glacier surface lowering over time. This limitation is particularly relevant for the tool-derived SLA observations, and the total and snow-covered area-elevation distributions, in addition to comparisons to field data. The 23 glaciers that were run twice with COPDEM and NASADEM indicate COPDEM tends to result in lower SLAs than NASADEM (SI Fig. 11). This difference likely represents surface lowering given the DEM reference dates (~2000 for NASADEM vs ~mid-2010s for COPDEM). We therefore suggest that elevations derived from observations that predate the DEM reference date be interpreted as minimum estimates, whereas those derived after the DEM reference date should be interpreted as maximum estimates.

Glacier surfaces are most easily classified from satellite imagery when glacier geometry is simple and when shadowing from surrounding topography, cloud cover, and debris cover are limited (e.g., Aberle and others, 2025). Challenges arise for glaciers with complex geometries (e.g., multiple tributaries, icefall(s), or steep ridgelines along the glacier margin), frequent cloudiness, extensive debris cover and topographic shadowing (e.g., Loibl and others, 2025). Because our tool is designed for global application, the workflow includes several features intended to manage these limitations as best as possible across a wide range of glacierized settings. Annual images are first filtered using user-defined thresholds for maximum cloud cover and minimum sun elevation, and scenes that do not meet these criteria are excluded. Further, the algorithm reduces topographic effects on reflectance using an Ekstrand correction based on terrain slope, aspect, and solar geometry. In addition, optional rock/water masking with user-selectable masking strength is provided to reduce misclassification of surrounding rock and water surfaces (including glacial lakes).

4.3. Use and value of the tool for glacier monitoring

4.3.1. Expansion of the observational record

Field-based glacier observations are often not continuous, even for well-monitored glaciers (e.g., Zemp and others, 2009). Our space-based approach substantially increases the methodological consistency and temporal availability of glacier health observations for field-monitored, as well as unmonitored glaciers. WGMS observations of TA and SCA are particularly sparse relative to ELA. Across the 40 years and 59 glaciers in our study, the tool provides ~800 additional observations of SCA and TA (equivalent to ~14 additional observations per glacier). This highlights the potential for space-based methods to complement in situ observations by improving the temporal completeness, and thus the overall quality, of glacier health records across multiple decades. However, we emphasize that tool-derived observations (1) are not equivalent to field-based WGMS measurements and are best interpreted as a complementary record rather than a direct replacement for missing in situ observations, and (2) are transient and do not necessarily represent end of balance year conditions (e.g., more direct comparisons would require sub-annual analysis). Thus, the tool may provide additional satellite-derived observations for years without WGMS measurements, but these are not equivalent to missing WGMS records and should not be used to gap fill missing years.

The tool is designed and intended for application beyond the relatively small number of well-monitored glaciers studied here and has the potential to generate accessible, multi-decadal observations for individual glaciers of interest that are currently unmonitored. Thus, in the following sections we discuss the potential value and application of the tool and workflow for academic and non-academic users while acknowledging known limitations and challenges.

4.3.2. Educational and non-academic use

Our tool is designed to support a wide range of users in gathering glacier health data for diverse applications, without the requirement of extensive coding knowledge or the internal structure of GEE. By removing these technical barriers to entry, the tool will make glaciological data more accessible across a range of educational and professional backgrounds. For example, we anticipate that this tool will be relevant in K-12 and higher education settings where it may be used to introduce students to concepts such as glacier and climate change, as well as Earth observation through hands-on exploration of remote sensing techniques.

We anticipate that our tool may also be relevant within communities that are highly dependent on glacial meltwater (e.g. the Andes) and where accessible glacier monitoring data remains limited, creating difficulties for local populations and policymakers attempting to adapt and mitigate the impacts of glacier loss (Vuille and others, 2018). However, we acknowledge that the tool may not perform equally well in all glacierized settings (e.g., when shadowing from surrounding topography, cloud cover, and debris cover are extensive) and that classification errors may occur. We therefore recommend that users visually inspect annual image and classification quality, assess the timing of observations relative to the end of the mass-balance year, and review outlying results before interpretation when applying the tool to individual glaciers of interest.

4.3.3. Academic use and potential for larger scale application

We expect that the application of the workflow may be valuable to a wide range of users across academic subfields (e.g. environmental assessment, water resource management, and hazard assessment), supporting site-specific data analyses where field observations are unavailable. For example, time series may be used to evaluate local glacier change and its implications for downstream ecosystems; trends in local glacier SCA and SLA may inform assessments of seasonal meltwater availability and variability; and changes in local glacier extent may provide context for identifying evolving conditions associated with glacier-related hazards.

The workflow presented here also holds potential for upscaling (i.e., regional and global glacier assessment) and, with the additional implementation of a sub-annual temporal dimension, could be useful for model comparison (e.g., Barandun et al., 2018). While sub-annual observations would be preferable for model application, the tool output does retain image acquisition dates. Thus, tool-derived observations may still be useful for transient intra-seasonal constraints and comparisons with model output. In addition, incorporation and use of other satellite missions could improve both the temporal and spatial resolution of glacier observations (e.g., Zeller and others, 2025) but doing so involves trade-offs. For example, Sentinel-2 does not provide the multi-decadal observational record afforded by Landsat and lacks the thermal band used in our workflow. Observational data are critically needed for the calibration and validation of glacier evolution models, and ultimately to improve projections of glacier change and its impacts. As noted by Wells and others (2025), observations of glacier change remain limited in both number and duration. Available records are sparse and relatively short compared to glacier response times and are therefore insufficient to robustly constrain model parameters. Regional and global application of the algorithm (with sub-annual observations) could substantially increase both the number and temporal range of glacier observations. However, we acknowledge and anticipate a number of challenges associated with large-scale application of the workflow. For example, selecting an appropriate month representative of the end of the mass balance year may be difficult for unmonitored glaciers (e.g., in tropical regions and for glaciers with summer accumulation). Further, difficulties may arise in regions with frequent or persistent cloud cover limiting the availability of suitable imagery. In addition, the tool has not been evaluated for heavily debris-covered glaciers. Finally, automated larger-scale (i.e., regional- and global-scaling) applications are likely not possible within the GEE platform and would require additional computing resources (e.g., high-performance computing).

In addition to integration and comparison with glacier evolution models, larger-scale and improved application of this workflow could enable assessment of the degree of glacier disequilibrium with the current climate state (via the AAR metric). This disequilibrium and the associated committed glacier mass loss during the twenty-first century remains poorly constrained (e.g., Marzeion and others, 2020). Expanded observational records could also help assess the representativeness of field-based time series used to extrapolate glacier change to mountain ranges lacking in situ observations (e.g., Zemp and others, 2009).

5. Conclusions

Here we present a novel cloud-based algorithm for the automatic classification of glacier surfaces and derivation of four transient glacier health metrics: snow-covered area (SCA), snowline altitude (SLA), total visible ice area (TA), and accumulation area ratio (AAR), all of which are closely related to climate and glacier mass balance. The tool is designed with accessibility in mind and can be applied to glaciers of interest, including those lacking in situ monitoring. We assessed the performance of the tool using 59 glaciers worldwide with long-term field-based observational records from the WGMS, as well as manually delineated observations for the same glaciers. After normalizing for glacier size and elevation range, we find overall good agreement between manual and tool-derived observations (SLA: $r = 0.73$, SCA: $r = 0.73$, TA $r = 0.59$, and AAR: $r = 0.79$), demonstrating the robustness of our automated image classification workflow. In contrast, agreement between WGMS and tool-derived observations is weak (SLA: $r = 0.20$, SCA: $r = 0.26$, TA $r = 0.22$, and AAR: $r = 0.18$), likely reflective of differences in methodology and observation date. Thus, tool-based glacier observations should be viewed as transient satellite-based observations that complement, rather than replace, field-based records. Across the 59 study glaciers, the tool generated ~800 additional observations of SCA and TA, substantially expanding observational coverage. We anticipate that the tool will be useful to a broad range of academic and non-academic users, including those with little to no coding or remote sensing experience. Future development of the workflow could incorporate a sub-temporal dimension, and larger-scale application could also provide critically needed multi-decadal observational records for calibration of glacier evolution models. In addition, application to individual glaciers could supply communities with accessible datasets to monitor nearby glaciers and respond effectively to ongoing glacier change.

Supplementary Material. The supplementary material for this article can be found at *insert link here*.

Data Availability Statement. The Glacier Health tool GUI and walkthrough instructions along with analysis results from the 59 study glaciers are available via GitHub at https://github.com/LamantiaKara/Glacier-Health-Tool. Supporting data are publicly available from the following sources: Glacier outlines (the glacier product and glacier complex product) are available from the Randolph Glacier Inventory version 7.0 (RGI7.0) at https://doi.org/10.5067/f6jmovy5navz (RGI Consortium, 2023); the ArcticDEM is available at https://doi.org/10.7910/DVN/3VDC4W (Porter and others, 2023); the Copernicus GLO-30 DEM is available at https://doi.org/10.5069/G9028PQB (European Space Agency, 2024), and Landsat imagery is available from the U.S. Geological Survey via several data portals (e.g., USGS EarthExplorer: https://earthexplorer.usgs.gov/).

Acknowledgements. This work was supported by a Royal Society Newton International Fellowship (NIFR1251037) to KAL. JML acknowledges support from UKRI Future Leaders Fellowship (MR/X02346X/1).

Author Contributions. All authors contributed to the methodology, based on initial ideas by KAL and LJL. KAL and JML wrote the Glacier Health tool code with input from LJL, FM, and RA. LJL and KAL wrote the first draft. All authors contributed to editing and revision.

Funding Statement. This research is funded by the Royal Society through the Newton International Fellowship (NIFR1251037).

Competing Interests. The authors declare that they have no competing interests.

References

Aberle R, Enderlin E, O'Neel S, Florentine C, Sass L, Dickson A and 2 others (2025) Automated snow cover detection on mountain glaciers using spaceborne imagery and machine learning. *The Cryosphere* **19**(4), 1675–1693.

Barandun M, Huss M, Usubaliev R, Azisov E, Berthier E, Kääb A, Bolch T and Hoelzle M (2018) Multi-decadal mass balance series of three Kyrgyz glaciers inferred from modelling constrained with repeated snow line observations. The Cryosphere 12(6), 1899–1919.

Baruah B, Rajak R, Gupta A, Sharma K, Roy A, Yadav S and 4 others (2026) Disappearing glaciers of Sikkim Himalaya: a multi-decadal remote sensing analysis. *Journal of Earth System Science* **135**(2), 80.

Benn D and Evans DJA (2010) *Glaciers and Glaciation*. Hodder Education, London.

Braithwaite RJ and Müller F (1980) On the parameterization of glacier equilibrium line altitude. *IAHS Publication* **126**, 263–271.

Calvin K, Dasgupta D, Krinner G, Mukherji A, Thorne PW, Trisos C and 16 others (2023) *IPCC, 2023: Climate Change 2023: Synthesis Report.* Contribution of Working Groups I, II and III to the Sixth Assessment Report of the Intergovernmental Panel on Climate Change, IPCC, Geneva, Switzerland.

Cogley JG, Hock R, Rasmussen LA, Arendt AA, Bauder A, Braithwaite RJ and 5 others (2011) *Glossary of Mass Balance and Related Terms*. IHP-VII Technical Documents in Hydrology No. 86, IACS Contribution No. 2.

Crippen, R., Buckley, S., Agram, P., Belz, E., Gurrola, E., Hensley, S., ... & Tung, W (2016) NASADEM global elevation model: Methods and progress. *The International Archives of the Photogrammetry, Remote Sensing and Spatial Information Sciences*, *41*, 125-128.

Dozier J (1989) Spectral signature of alpine snow cover from the Landsat Thematic Mapper. *Remote Sensing of Environment* **28**, 9–22.

Durán-Alarcón C, Gevaert CM, Mattar C, Jiménez-Muñoz JC, Pasapera-Gonzales JJ, Sobrino JA and 4 others (2015) Recent trends on glacier area retreat over the group of Nevados Caullaraju-Pastoruri (Cordillera Blanca, Peru) using Landsat imagery. *Journal of South American Earth Sciences* **59**, 19–26.

Ekstrand S (1996) Landsat TM-based forest damage assessment: correction for topographic effects. *Photogrammetric Engineering and Remote Sensing* **62**(2), 151–161.

European Space Agency (2024) Copernicus Global Digital Elevation Model [dataset]. Distributed by OpenTopography. (doi:10.5069/G9028PQB). Accessed 28 January 2026.

Ficetola GF, Marta S, Guerrieri A, Cantera I, Bonin A, Cauvy-Fraunié S and 10 others (2024) The development of terrestrial ecosystems emerging after glacier retreat. *Nature* **632**(8024), 336–342.

Haeberli W and Whiteman C (2015) Snow and ice-related hazards, risks, and disasters: a general framework. In Haeberli W and Whiteman C (eds.), *Snow and Ice-Related Hazards, Risks, and Disasters*, Academic Press, 1–34.

Hall DK and Riggs GA (2010) Normalized-difference snow index (NDSI). In Singh VP, Singh P and Haritashya UK (eds.), *Encyclopedia of Snow, Ice and Glaciers*, Springer.

Hock R, Bliss A, Marzeion B, Giesen RH, Hirabayashi Y, Huss M and 2 others (2019) GlacierMIP – a model intercomparison of global-scale glacier mass-balance models and projections. *Journal of Glaciology* **65**(251), 453–467.

Hugonnet R, McNabb R, Berthier E, Menounos B, Nuth C, Girod L and 5 others (2021) Accelerated global glacier mass loss in the early twenty-first century. *Nature* **592**(7856), 726–731.

Huss M and Hock R (2018) Global-scale hydrological response to future glacier mass loss. *Nature Climate Change* **8**(2), 135–140.

Huss M, Fischer M, Linsbauer A and Bauder A (2025) Continuous monitoring of a glacier's extinction. *Annals of Glaciology* **66**, e27.

Immerzeel WW, Lutz AF, Andrade M, Bahl A, Biemans H, Bolch T and 14 others (2020) Importance and vulnerability of the world's water towers. *Nature* **577**(7790), 364–369.

Krajčí, P., Holko, L., Perdigão, R. A., & Parajka, J (2014) Estimation of regional snowline elevation (RSLE) from MODIS images for seasonally snow covered mountain basins. *Journal of hydrology*, *519*, 1769-1778.

Larocca LJ, Twining-Ward M, Axford Y, Schweinsberg AD, Larsen SH, Westergaard-Nielsen A and 4 others (2023) Greenland-wide accelerated retreat of peripheral glaciers in the twenty-first century. *Nature Climate Change* **13**(12), 1324–1328.

Larocca LJ, Lea JM, Erb MP, McKay NP, Phillips M, Lamantia KA and Kaufman DS (2024) Arctic glacier snowline altitudes rise 150 m over the last 4 decades. *The Cryosphere* **18**(8), 3591–3611.

Loibl D, Richter N and Grünberg I (2025) Remote sensing-derived time series of transient glacier snowline altitudes for High Mountain Asia, 1985–2021. *Scientific Data* **12**(1), 103.

Malca UFG, Solano LNY, Carranza SVC, Alvarez DGC, Quispe FCQ, García JAC and Mark BG (2025) The loss of glacier resilience due to climate change throughout the Cordillera Blanca, Peru between 1984 and 2023. *Quaternary Science Advances* **19**, 100286.

Marzeion B, Hock R, Anderson B, Bliss A, Champollion N, Fujita K and 9 others (2020) Partitioning the uncertainty of ensemble projections of global glacier mass change. *Earth's Future* **8**(7), e2019EF001470.

Masson-Delmotte V, Zhai P, Pirani A, Connors SL, Péan C, Berger S and 6 others (2021) *Climate Change 2021: The Physical Science Basis.* Contribution of Working Group I to the Sixth Assessment Report of the Intergovernmental Panel on Climate Change, Cambridge University Press.

Meier MF (1962) Proposed definitions for glacier mass budget terms. *Journal of Glaciology* **4**(33), 252–263.

Mernild SH, Pelto M, Malmros JK, Yde JC, Knudsen NT and Hanna E (2013) Identification of snow ablation rate, ELA, AAR and net mass balance using transient snowline variations on two Arctic glaciers. *Journal of Glaciology* **59**(216), 649–659.

Moussavi M, Pope A, Halberstadt ARW, Trusel LD, Cioffi L and Abdalati W (2020) Antarctic supraglacial lake detection using Landsat 8 and Sentinel-2 imagery: towards continental generation of lake volumes. *Remote Sensing* **12**(1), 134.

Ohmura A and Boettcher M (2022) On the shift of glacier equilibrium line altitude (ELA) under the changing climate. *Water* **14**(18), 2821.

Otosaka IN, Shepherd A, Ivins ER, Schlegel NJ, Amory C, van den Broeke M and 6 others (2022) Mass balance of the Greenland and Antarctic ice sheets from 1992 to 2020. *Earth System Science Data Discussions 2022*, 1–33.

Otsu N (1979) A threshold selection method from gray-level histograms. *IEEE Transactions on Systems, Man, and Cybernetics* **9**(1), 62–66.

Pfeffer WT, Arendt AA, Bliss A, Bolch T, Cogley JG, Gardner AS and 11 others (2014) The Randolph Glacier Inventory: a globally complete inventory of glaciers. *Journal of Glaciology* **59** (221), 537–552.

Porter C, Howat I, Noh MJ, Husby E, Khuvis S, Danish E and others (2023) ArcticDEM – Mosaics, Version 4.1 [dataset]. Harvard Dataverse. (doi:10.7910/DVN/3VDC4W).

Rabatel A, Bermejo A, Loarte E, Soruco A, Gomez J, Leonardini G and 2 others (2012) Can the snowline be used as an indicator of the equilibrium line and mass balance for glaciers in the outer tropics? *Journal of Glaciology* **58**(212), 1027–1036.

Rabatel A, Letréguilly A, Dedieu JP and Eckert N (2013) Changes in glacier equilibrium-line altitude in the western Alps from 1984 to 2010: evaluation by remote sensing and modeling of the morpho-topographic and climate controls. *The Cryosphere* **7**(5), 1455–1471.

Racoviteanu AE, Rittger K and Armstrong R (2019) An automated approach for estimating snowline altitudes in the Karakoram and Eastern Himalaya from remote sensing. *Frontiers in Earth Science* **7**, 220.

Ramírez E, Francou B, Ribstein P, Descloitres M, Guérin R, Mendoza J and 4 others (2001) Small glaciers disappearing in the tropical Andes: a case-study in Bolivia: Glaciar Chacaltaya (16°S). *Journal of Glaciology* **47**(157), 187–194.

Rastner P, Prinz R, Notarnicola C, Nicholson L, Sailer R, Schwaizer G and Paul F (2019) On the automated mapping of snow cover on glaciers and calculation of snow line altitudes from multi-temporal Landsat data. *Remote Sensing* **11**(12), 1410.

RGI Consortium (2023) Randolph Glacier Inventory – A Dataset of Global Glacier Outlines (NSIDC-0770, Version 7) [dataset]. National Snow and Ice Data Center, Boulder, Colorado, USA. (doi:10.5067/F6JMOVY5NAVZ). Accessed 27 January 2026.

Riggs GA, Hall DK and Salomonson VV (1994) A snow index for the Landsat Thematic Mapper and Moderate Resolution Imaging Spectroradiometer. *Proceedings of IGARSS'94 – 1994 IEEE International Geoscience and Remote Sensing Symposium* **4**, 1942–1944.

Rounce DR, Hock R, Maussion F, Hugonnet R, Kochtitzky W, Huss M and 6 others (2023) Global glacier change in the 21st century: every increase in temperature matters. *Science* **379**(6627), 78–83.

Santofimia E, López-Pamo E, Palomino EJ, González-Toril E and Aguilera Á (2017) Acid rock drainage in Nevado Pastoruri glacier area (Huascarán National Park, Perú): hydrochemical and mineralogical characterization and associated environmental implications. *Environmental Science and Pollution Research* **24**(32), 25243–25259.

Schuster L, Rounce DR and Maussion F (2023) Glacier projections sensitivity to temperature-index model choices and calibration strategies. *Annals of Glaciology* **64**(92), 293–308.

Serrano RB, Soria A, Cusicanqui D, Rojas S, Torres G, Rivadeneira A and 3 others (2026) In memory of Carihuairazo, a recently disappeared ice cap in the inner tropics. *Annals of Glaciology* **67**, e14.

Stillinger, T., Roberts, D. A., Collar, N. M., & Dozier, J. (2019) Cloud masking for Landsat 8 and MODIS Terra over snow-covered terrain: Error analysis and spectral similarity between snow and cloud. *Water Resources Research*, *55*(7), 6169-6184.

The GlaMBIE Team (2025) Community estimate of global glacier mass changes from 2000 to 2023. *Nature* **639**, 382–388. (doi:10.1038/s41586-024-08545-z).

Van Tricht L, Zekollari H, Huss M, Rounce DR, Schuster L, Aguayo R and 4 others (2025) Peak glacier extinction in the mid-twenty-first century. *Nature Climate Change*, 1–5. (doi: 10.1038/s41558-025-02513-9)

Vuille M, Carey M, Huggel C, Buytaert W, Rabatel A, Jacobsen D and 6 others (2018) Rapid decline of snow and ice in the tropical Andes – impacts, uncertainties and challenges ahead. *Earth-Science Reviews* **176**, 195–213.

Warren SG (2019) Optical properties of ice and snow. *Philosophical Transactions of the Royal Society A: Mathematical, Physical and Engineering Sciences* **377**(2146).

Wells A, Tober BS, Child SF, Rounce DR, Loso MG, Hults CP and 4 others (2025) An 85-year record of glacier change and refined projections for Kennicott and Root Glaciers, Alaska. *Nature Communications* **16**(1), 7835.

WGMS (2023) *Global Glacier Change Bulletin No. 5 (2020–2021)*. Zemp M, Gärtner-Roer I, Nussbaumer SU, Welty EZ, Dussaillant I and Bannwart J (eds.). World Glacier Monitoring Service, Zurich, Switzerland. (doi:10.5904/wgms-fog-2023-09).

WGMS (2024) Fluctuations of Glaciers Database [dataset]. World Glacier Monitoring Service, Zurich, Switzerland. (doi:10.5904/wgms-fog-2024-01).

Zeller L, McGrath D, Sass L, Florentine C and Downs J (2025) Equilibrium line altitudes, accumulation areas and the vulnerability of glaciers in Alaska. *Journal of Glaciology* 71, e28.

Zemp M, Hoelzle M and Haeberli W (2009) Six decades of glacier mass-balance observations: a review of the worldwide monitoring network. *Annals of Glaciology* **50**(50), 101–111.

Zhu, Z., Wang, S., & Woodcock, C. E. (2015) Improvement and expansion of the Fmask algorithm: Cloud, cloud shadow, and snow detection for Landsats 4–7, 8, and Sentinel 2 images. *Remote sensing of Environment*, *159*, 269-277.

Figure Captions

Figure 1. Global glacier locations (pink polygons) and locations of the 59 field-monitored glaciers from the World Glacier Monitoring Service (WGMS) used for tool validation and error estimation (black dots). Shaded polygons with thin gray edges represent the 19 first-order regions of the Randolph Glacier Inventory (RGI version 7.0; RGI Consortium, 2023).

Figure 2. Indicators of glacier health included in the tool. The snow-covered area (SCA; 1); the snowline altitude (SLA; 2); the ablation area (3), the total visible ice area (TA; 1+3); and the accumulation-area ratio (AAR; 1/(1+3)).

Figure 3. Flowchart of the tool's workflow noting each step in the imagery collection and analysis process. Further details and the workflow code are available in the GitHub repository.

Figure 4. Imagery acquisition month relative to the target month for each of the study glaciers over the 1985–2024 observation period with a maximum image cloud cover threshold of 20%. White squares denote the target month, with a color gradient indicating the number of images acquired per month (left), and a bar chart showing the percentage of images within the target month relative to the total number of acquired images (right).

Figure 5. Example outputs for the Gulkana Glacier, Alaska, August 22, 2021 (Landsat 8). (a) Histogram of Ekstrand-corrected NIR surface reflectance (unitless) for a single end-of-summer Landsat scene, with the Otsu-derived threshold (yellow line) separating the bimodal distribution of snow (red) and ice (blue). (b) Resulting delineations of total visible ice area (TA; blue) and snow-covered area (SCA; red) used in subsequent calculations of AAR and SLA.

Figure 6. Comparison of the tool–derived glacier health metrics with manually digitized values (top row; panels a–d) and WGMS observations (bottom row; panels e–h). Metrics shown include snowline altitude/equilibrium-line altitude (SLA/ELA), snow-covered area (SCA), total glacier area (TA), and accumulation-area ratio (AAR). SLA/ELA is expressed as an anomaly (m) relative to each glacier's median tool-derived SLA. SCA and TA are expressed as ratios relative to each glacier's median tool-derived values to reduce the influence of between-glacier differences in size. AAR is shown in raw unitless form. Solid gray lines show the 1:1 relationship, dashed black lines show linear regression fits.

Figure 7. Comparison of tool-derived (pink) and WGMS-derived (blue) glacier health metrics: temporal changes and relationships with annual mass balance. (a–c) Temporal changes in glacier health metrics: (a) total area (TA), (b) snow-covered area (SCA; accumulation area for WGMS), and (c) snowline altitude (SLA; equilibrium-line altitude [ELA] for WGMS). Annual median values across all glaciers are shown as solid lines, with shading indicating the interquartile range (IQR). For TA and SCA, values are expressed as percent change relative to each glacier's median value during 1985–2024. For SLA/ELA, values are expressed as anomalies relative to each glacier's median 1985–2024 SLA/ELA. (d–f) Distribution of glacier-level Pearson correlation coefficients (r) between annual mass balance and (d) TA, (e) SCA (accumulation area for WGMS), and (f) SLA (ELA for WGMS). Colored dashed lines indicate the median r value for each dataset.

Formatted Tables

Table 1. Imagery acquisition parameters and processing options

Panel Heading	Input Variable	Options
Collect Imagery	Glacier Name	Any (e.g. Gulkana)
	Start Year	1985 to Present Year
	End Year	1985 to Present Year
	Target Month	January through December (1-12)
	Max Cloud Cover	0 to 100% (increments of 5)
	Min Sun Angle	0 to 90 degrees (increments of 5)
Processing Options	DEM Source	COPDEM, NASADEM, or Arctic DEM
	Rock/Water Masking Strength	'Off', 'Light', 'Moderate', or 'High'

Table 2. Validation and uncertainty of tool-derived glacier health metrics

	Tool versus Field Obs. (WGMS)						Tool versus Manual Satellite Obs.					
Metric	*n*	Bias	RMSE	MAE	*r*	Median abs % diff	*n*	Bias	RMSE	MAE	*r*	Median abs % diff
SLA/ELA (m)	1154	-112	211	156	0.20	5	216	18.5	83.3	49.2	0.73	1
SCA (km^2)	557	2.1	9.7	2.8	0.26	46	217	-1.0	6.8	1.6	0.73	10
TA (km^2)	557	0.4	6.0	1.4	0.22	9	216	-1.5	8.7	1.9	0.59	5

Validation statistics for the tool-derived glacier health metrics compared with field-based observations (left) and manual digitizations (right). *n* denotes the number of paired observations; RMSE is the root-mean-square error; MAE is the mean absolute error; *r* is the Pearson correlation coefficient; and Median abs % diff is the median absolute percent difference (%). AAR is not included because it is derived from SCA and TA. Statistics were computed using the post-processed dataset. Pearson correlation coefficients were calculated using glacier-specific normalized or anomaly values to account for differences in glacier size and elevation.

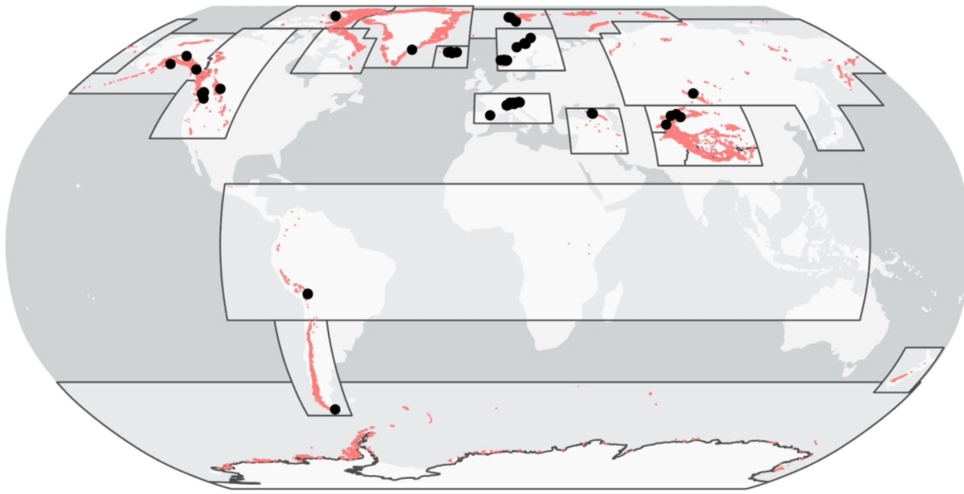

Figure 1. Global glacier locations (pink polygons) and locations of the 59 field-monitored glaciers from the World Glacier Monitoring Service (WGMS) used for tool validation and error estimation (black dots). Shaded polygons with thin gray edges represent the 19 first-order regions of the Randolph Glacier Inventory (RGI version 7.0; RGI Consortium, 2023).

240x127mm (300 x 300 DPI)

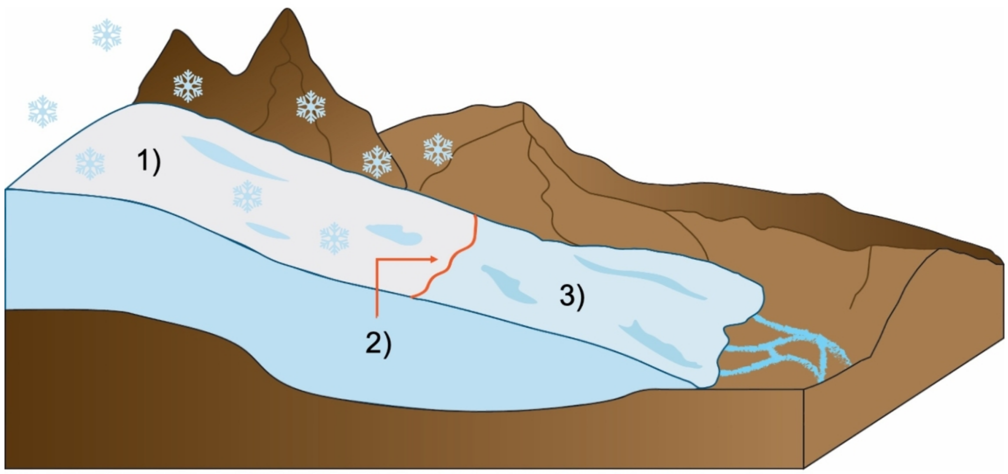

Figure 2. Indicators of glacier health included in the tool. The snow-covered area (SCA; 1); the snowline altitude (SLA; 2); the ablation area (3), the total visible ice area (TA; 1+3); and the accumulation-area ratio (AAR; 1/(1+3)).

338x190mm (144 x 144 DPI)

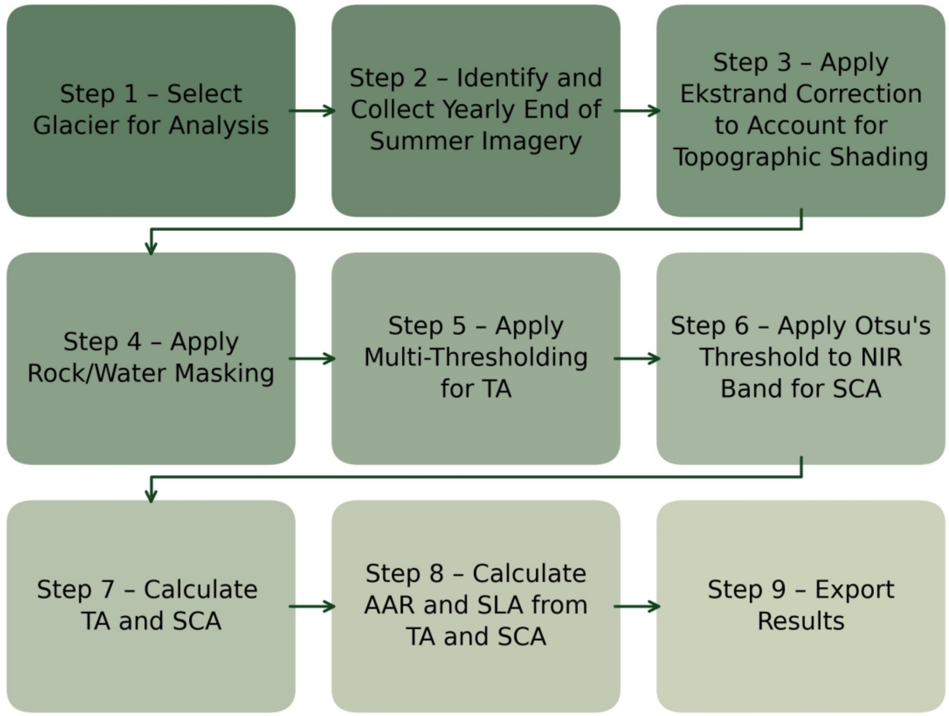

Figure 3. Flowchart of the tool's workflow noting each step in the imagery collection and analysis process. Further details and the workflow code are available in the GitHub repository.

201x153mm (300 x 300 DPI)

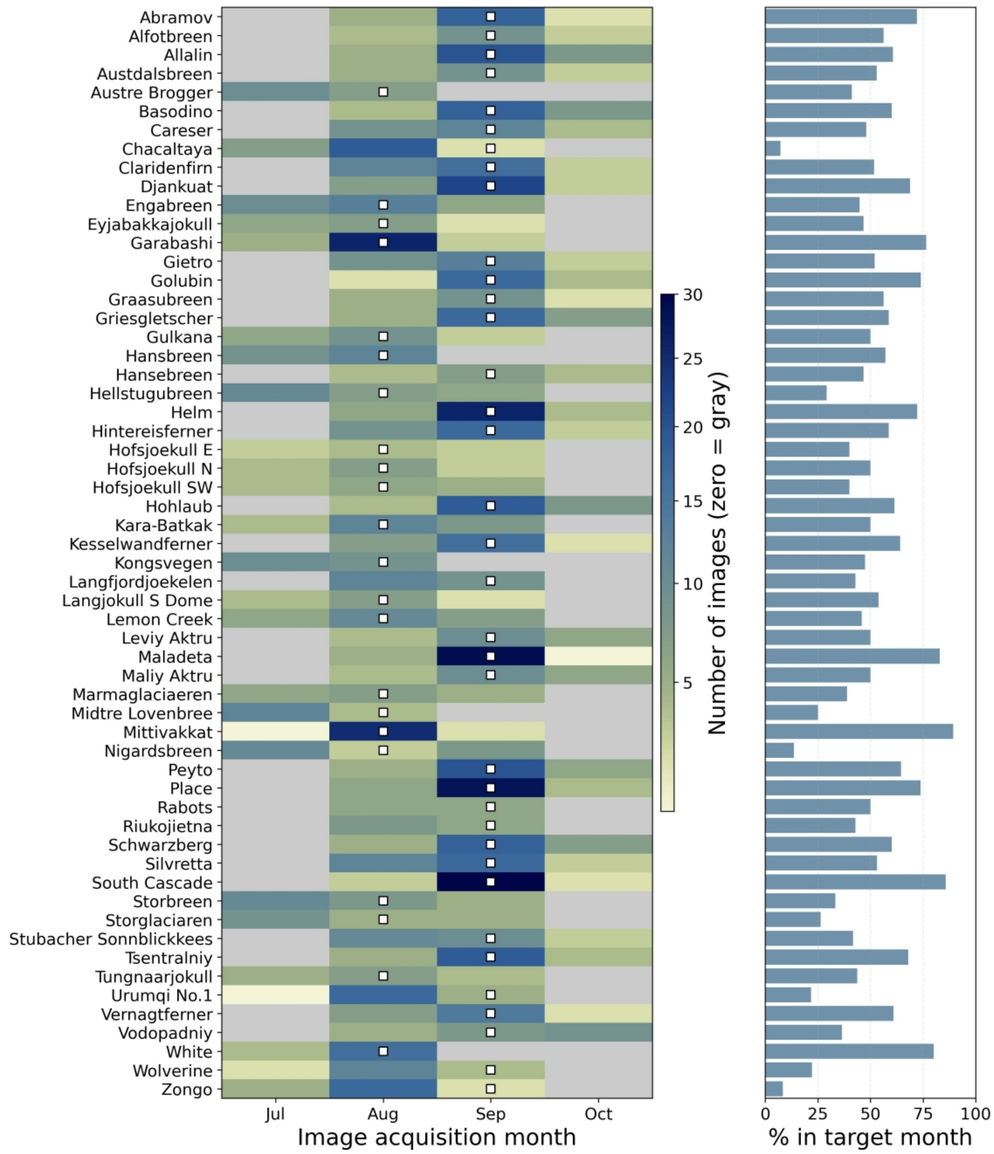

Figure 4. Imagery acquisition month relative to the target month for each of the study glaciers over the 1985–2024 observation period with a maximum image cloud cover threshold of 20%. White squares denote the target month, with a color gradient indicating the number of images acquired per month (left), and a bar chart showing the percentage of images within the target month relative to the total number of acquired images (right).

282x326mm (300 x 300 DPI)

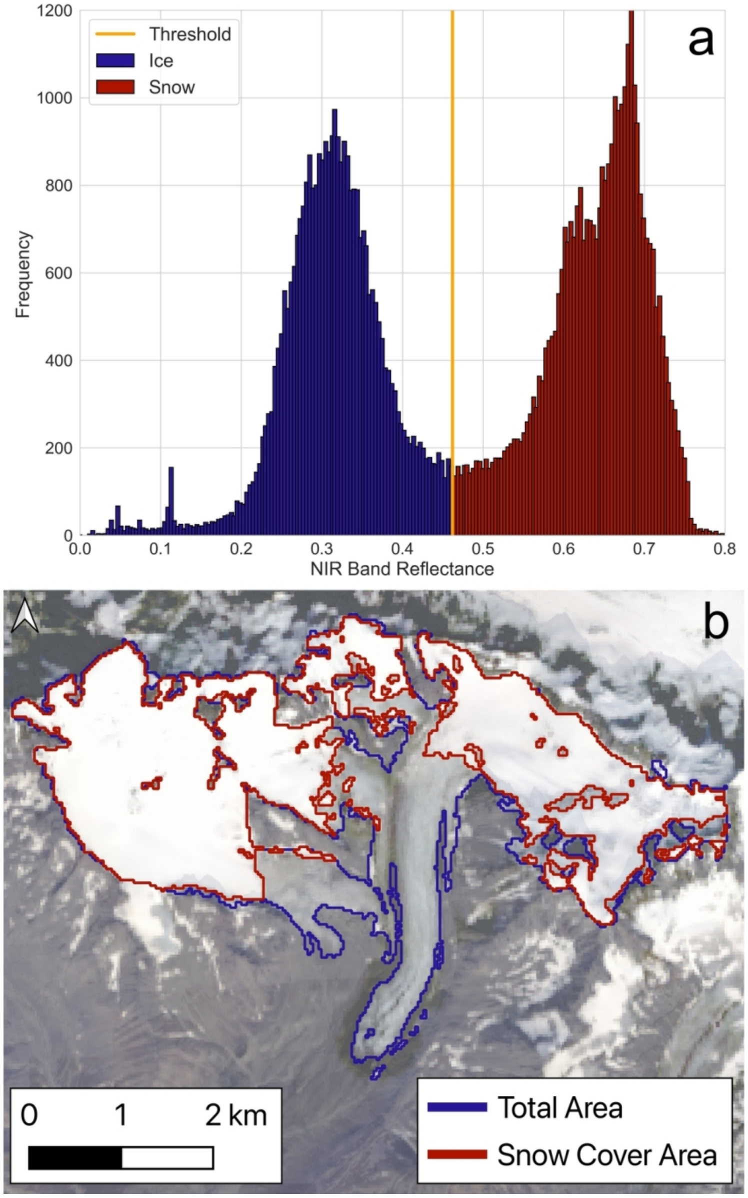

Figure 5. Example outputs for the Gulkana Glacier, Alaska, August 22, 2021 (Landsat 8). (a) Histogram of Ekstrand-corrected NIR surface reflectance (unitless) for a single end-of-summer Landsat scene, with the Otsu-derived threshold (yellow line) separating the bimodal distribution of snow (red) and ice (blue). (b) Resulting delineations of total visible ice area (TA; blue) and snow-covered area (SCA; red) used in subsequent calculations of AAR and SLA.

102x165mm (300 x 300 DPI)

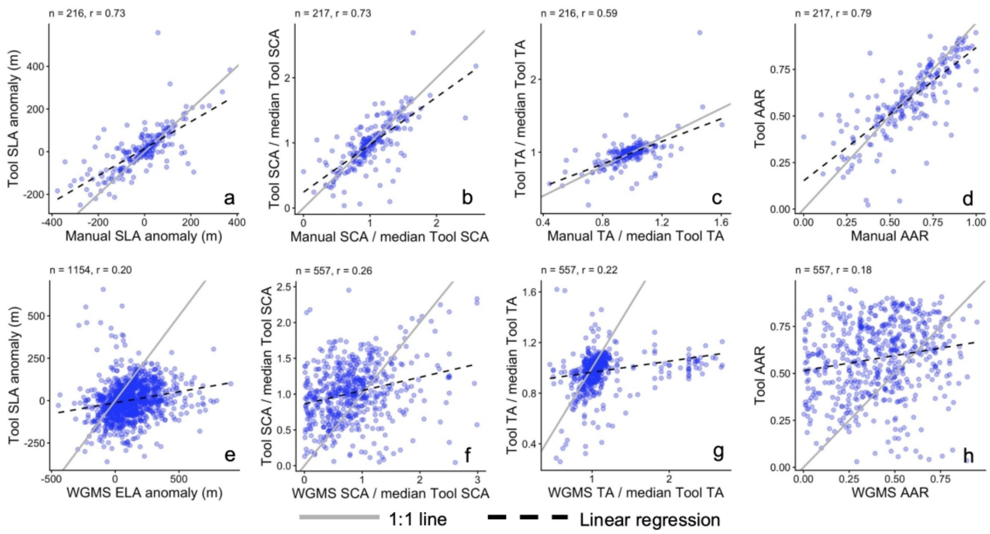

Figure 6. Comparison of the tool–derived glacier health metrics with manually digitized values (top row; panels a–d) and WGMS observations (bottom row; panels e–h). Metrics shown include snowline altitude/equilibrium-line altitude (SLA/ELA), snow-covered area (SCA), total glacier area (TA), and accumulation-area ratio (AAR). SLA/ELA is expressed as an anomaly (m) relative to each glacier's median tool-derived SLA. SCA and TA are expressed as ratios relative to each glacier's median tool-derived values to reduce the influence of between-glacier differences in size. AAR is shown in raw unitless form. Solid gray lines show the 1:1 relationship, dashed black lines show linear regression fits.

1285x693mm (72 x 72 DPI)

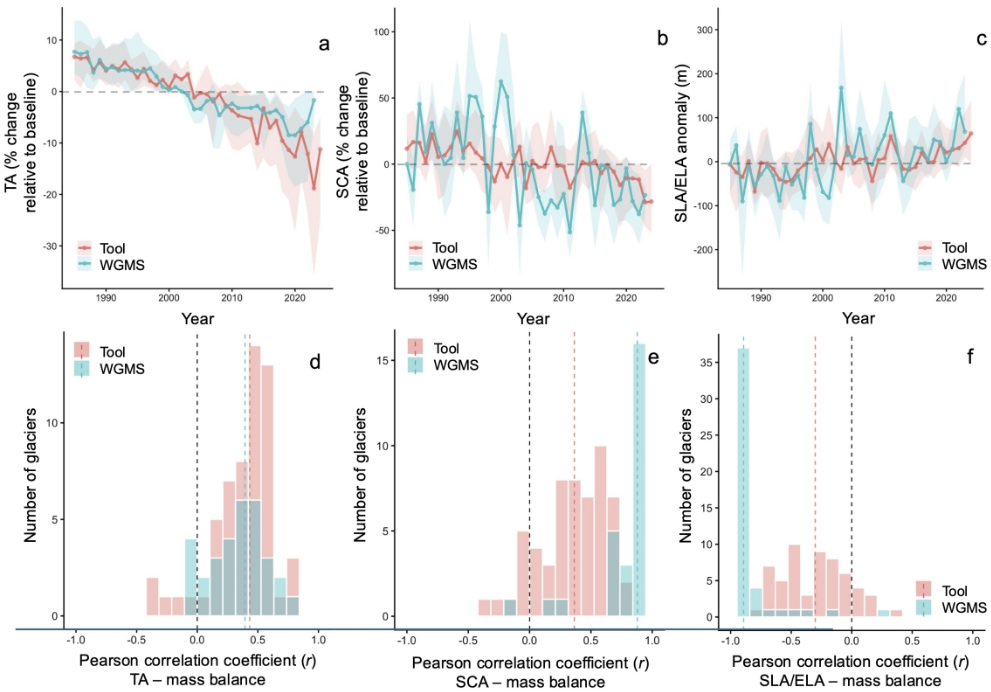

Figure 7. Comparison of tool-derived (pink) and WGMS-derived (blue) glacier health metrics: temporal changes and relationships with annual mass balance. (a–c) Temporal changes in glacier health metrics: (a) total area (TA), (b) snow-covered area (SCA; accumulation area for WGMS), and (c) snowline altitude (SLA; equilibrium-line altitude [ELA] for WGMS). Annual median values across all glaciers are shown as solid lines, with shading indicating the interquartile range (IQR). For TA and SCA, values are expressed as percent change relative to each glacier's median value during 1985–2024. For SLA/ELA, values are expressed as anomalies relative to each glacier's median 1985–2024 SLA/ELA. (d–f) Distribution of glacier-level Pearson correlation coefficients (r) between annual mass balance and (d) TA, (e) SCA (accumulation area for WGMS), and (f) SLA (ELA for WGMS). Colored dashed lines indicate the median r value for each dataset.

1272x877mm (72 x 72 DPI)